AIAA 80-1424R

Nonequilibrium Flow over Delta Wings with Detached Shock Waves

R. J. Stalker*
University of Queensland, Brisbane, Australia

An analysis is made of the effect of streamwise density changes, due to chemical reactions, on the flow in the shock layer of a medium- to low-aspect-ratio delta wing at angles of incidence such that the shock wave is detached from the leading edges. It is shown that the flow retains the essentially conical character that is associated with the absence of density changes. Near the midspan of the wing, the density changes displace the shock wave toward the wing surface but do not alter the shock shape. The displacement effect predicted by the analysis is confirmed by experiments in a high-enthalpy shock tunnel.

Nomenclature

A	= constant defined following Eq. (24)
b	= semispan per unit length
C	$= -h/b\epsilon^{1/2}$
h	= ridgeline height per unit length
H_2	= enthalpy downstream of shock
H_s	= stagnation enthalpy
H_∞	= enthalpy upstream of shock
K	= reaction constant
l	= chordwise length of wing
p	= absolute pressure
q	= resultant velocity downstream of shock
U	= mainstream velocity
u,v,w	= nondimensional velocity components
x^*	= distance from wing apex
y^*,z^*	= associated Cartesian coordinates
x,y,z	= conical coordinates
x,z,η	= modified coordinates
y_{s0}	= centerline shock coordinate in constant-density flow
$(y_s-y)_0$	= distance from shock to streamline in constant-density flow
α	= angle of incidence
δ/x^*	= normalized midspan shock standoff
Δ_0	= shock standoff from ridgeline in y coordinates
Δy	= streamline displacement due to relaxation
Δy_b	= surface displacement due to relaxation
ϵ	$= (=\rho_\infty/\rho_s)$, inverse shock-density ratio
ρ	= density
σ^*	= distance from shock along streamline
σ	$= \sigma^*/l$
σ'	$= \sigma/x$
ϕ	$= [=(\rho/\rho_s-1)]$, density variable
χ	= binary reaction parameter
Ω	$= b/(\epsilon^{1/2}\tan\alpha)$

Subscripts

b	= body
f	= frozen
e	= equilibrium
s	= shock
∞	= upstream of shock

Presented as Paper 80-1424 at the AIAA 13th Fluid and Plasma Dynamics Conference, Snowmass, Colo., July 14-16, 1980; submitted Sept. 19, 1981; revision received Nov. 16, 1981.

*Professor of Mechanical Engineering. Member AIAA.

I. Introduction

WHEN a medium- to low-aspect-ratio delta wing with sharp leading edges flies at high supersonic speeds, a shock wave is formed on the windward side of the wing. At all but low angles of incidence, the shock is attached to the leading edges only at the wing apex. The resulting shock-layer flow has been subject to a number of theoretical and experimental investigations[1-5] for cases in which the density of the fluid in the layer remains essentially constant.

However, at flight conditions associated with gliding reentry from Earth orbit, chemical reactions cause significant density changes within the shock layer. The problem of incorporating these density changes within delta wing shock-layer theory is considered in this paper. The conical-flow theory originated by Messiter[1] for constant-density flows, and extended by Hillier to nearly conical flows, is further extended to accommodate the density changes arising from chemical relaxation. The effect of these changes is then determined as a perturbation of the constant-density results presented by Squire.[3] The theory is compared with exact numerical calculations and with experimental results in the form of measurements, made by Stollery and Stalker,[6,7] of shock standoff on delta wings in a high-enthalpy shock tunnel.

II. Analysis

A. Flow Equations

The flow configuration is shown in Fig. 1. The wing has a delta planform. The shock wave, which is attached only at the wing apex, bounds a thin shock layer that is formed on the wing. The reference plane is taken to be in the plane of the wing leading edges at the apex, and the angle of incidence α is taken as the angle between the incident flow direction and the line $00'$ through the midspan of the wing in the reference plane. Curvature of the wing surface in the crossflow plane (i.e., the x^*, z^* plane) is allowable, provided that the radius of curvature is large in comparison with the span.

The flow analyzed by Messiter[1] and others who followed him[3,4] involved a conical wing, with a conical flow in the shock layer and a shock wave that is a ruled surface, with the generators passing through the wing apex. Hillier[2] showed that these requirements for a strictly conical flow configuration can be relaxed, and that the flow can be analyzed for more general configurations in which the leading edges are not necessarily straight and in which both the shock and the wing surface may exhibit curvature in the streamwise direction.

Hillier began by defining Cartesian coordinates x^*, y^*, z^*, with the x^* and z^* coordinates located in the reference plane

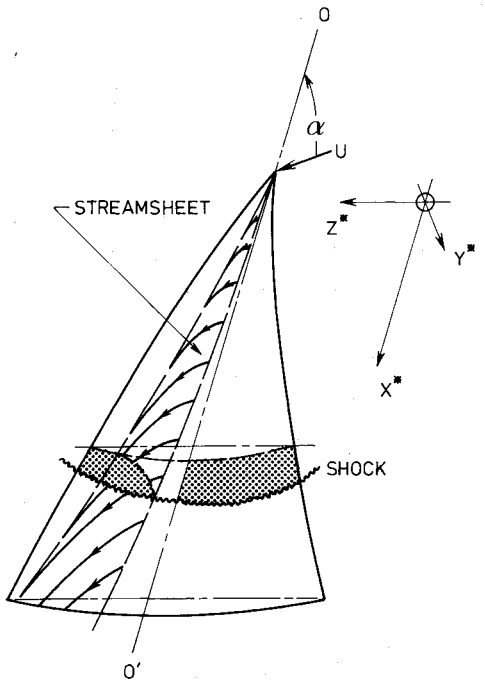

Fig. 1 Typical configuration.

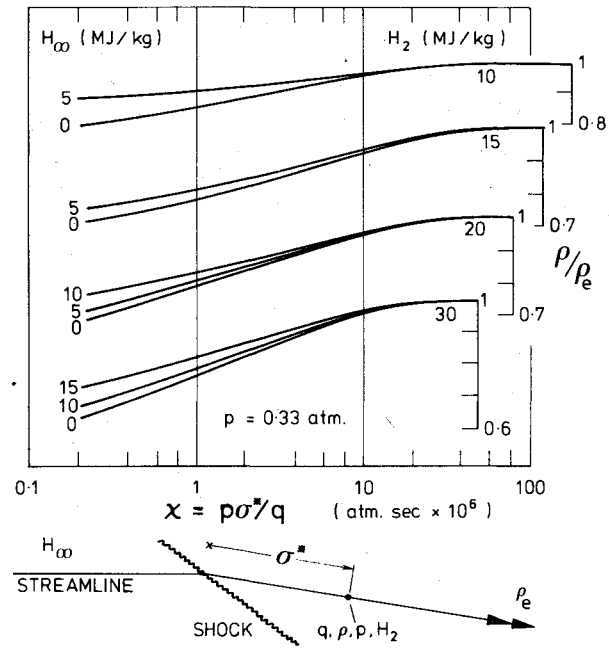

Fig. 2 Constant pressure relaxation downstream of shock in air.

and y^* directed away from the wing surface. Velocity components were taken as u^*, v^*, and w^* in the x^*, y^*, and z^* directions, respectively. He employed the transformations

$$x=x^*/l, \quad y=y^*/(x^*\epsilon\tan\alpha), \quad z=z^*/(x^*\epsilon^{1/2}\tan\alpha) \tag{1a}$$

$$u=(u^*/U-\cos\alpha)/(\epsilon\sin\alpha\tan\alpha), \quad v=v^*/(U\epsilon\sin\alpha)$$

$$w=w^*/(U\epsilon^{1/2}\sin\alpha) \tag{1b}$$

to develop the equations of flow in the shock layer, and, by neglecting terms of order ϵ, where $\epsilon \ll 1$, he obtained the thin-shock-layer equations in conical coordinates. He then assigned the coordinate y the role of a dependent variable and introduced a new independent variable η defining an arbitrary streamsheet that originated at the apex of the wing, as shown in Fig. 1. Now, a property of the flow that emerges from the thin-shock-layer equations is that w is constant along streamlines within the shock layer and therefore, if the streamsheet is chosen such that w is constant along the trace of the streamsheet at the shock, then w is constant over all of the streamsheet. By using this condition, Hillier obtained the continuity equation in the shock layer in a form that allows it to be formally integrated.

Hillier's analysis can be extended readily to the case where density changes within the shock layer are of the same order as the density at the shock. The continuity relation then yields the equation

$$x\frac{\partial^2 y}{\partial x\partial\eta}+[w(\eta)-z]\frac{\partial^2 y}{\partial z\partial\eta}=-\frac{\partial y}{\partial\eta}\left(1+\frac{x^*}{1+\phi}\frac{\mathrm{D}\phi}{\mathrm{D}\sigma^*}\right) \tag{2a}$$

when it is combined with the differential equation for the streamlines, i.e.,

$$y-v+x(\partial y/\partial x)+[w(\eta)-z](\partial y/\partial z)=0 \tag{2b}$$

Here $\rho=\rho_s(1+\phi)$, and $\mathrm{D}\phi/\mathrm{D}\sigma^*$ signifies differentiation of ϕ along a streamline. For constant density, Eq. (2a) reduces to Eq. (6.1) of Hillier. Equations (2a) and (2b) are associated with the shock boundary conditions

$$v_s=y_s+x(\partial y_s/\partial x)-1-(\partial y_s/\partial z)^2-z(\partial y_s/\partial z) \tag{2c}$$

$$w_s=-\partial y_s/\partial z \tag{2d}$$

and the boundary conditions at the body

$$(\partial y/\partial x)_{\text{body}}=\partial y_B/\partial x_B, \qquad (\partial y/\partial z)_{\text{body}}=\partial y_B/\partial z_B \tag{2e}$$

The preceding equations are sufficient to define the crossflow in the shock layer.

B. The Reaction Term

The effect of chemical reactions on the density is contained in the last term in the parentheses on the right-hand side of Eq. (2a). Neglecting terms of $0(\epsilon)$, it is possible to write

$$\sigma^*=x^*-x_s^* \tag{3}$$

and if it is also noted that w^* is constant along streamlines, then

$$z^*-z_s^*=(x^*-x_s^*)\,w^*/U\cos\alpha$$

or, using the transformations (1a) and (1b),

$$x^*/(x^*-x_s^*)=\{[w(\eta)-z_s]/(z-z_s)\}_{\eta_s} \tag{4}$$

where the braces about the term on the right-hand side serve as a reminder that the relation applies along a streamline originating at the shock. Thus it is found that

$$\frac{x^*}{1+\phi}\frac{\mathrm{D}\phi}{\mathrm{D}\sigma^*}=\left[\frac{w(\eta)-z_s}{z-z_s}\right]_{\eta_s}\frac{\mathrm{D}[\ln(1+\phi)]}{\mathrm{D}(\ln\sigma^*)} \tag{5}$$

where z_s is the value of z at which the streamline meets the shock.

Now, the pressure changes within the shock layer are small, and so it is a good approximation to assume that reactions take place at constant pressure along streamlines. Thus, the variation of density with distance from the shock will follow curves of the type shown in Fig. 2. These curves were

calculated for air by following the method of Ref. 8. They display the variation of density due to chemical relaxation, expressing the density as a fraction of the equilibrium density ρ_e that is achieved far downstream and distance from the shock in terms of the binary reaction parameter χ. The curves have been obtained for $p=33$ kNm^{-2}, corresponding approximately to the test conditions of Stollery and Stalker. Over a large range of pressures, however, the slope of these curves is independent of the pressure level.

The variation of $\ell n(1+\phi)$ with $\ell n\sigma^*$ follows curves of the same form, as shown in Fig. 3a. This curve can be modeled by a ramp function, as shown by the broken lines in the figure, and this allows

$$\frac{D[\ell n(1+\phi)]}{D(\ell n\sigma^*)}$$

to be represented by a step function, as shown in Fig. 3b. According to the model, the derivative is zero while the gas remains frozen, up to distance σ_f^* from the shock, and suddenly increases to K, the slope of the broken line in Fig. 3a, as the gas begins to react. The derivative remains at this value until the gas reaches the equilibrium condition, at distance σ_e^* from the shock, when the derivative drops to zero again. Inserting this step function into Eq. (5) and using it to substitute in Eq. (2a), Eq. (2a) becomes

$$[w(\eta)-z]\frac{\partial^2 y}{\partial z\partial\eta}+x\frac{\partial^2 y}{\partial x\partial\eta}=-\frac{\partial y}{\partial\eta}\left\{1+\left(\frac{w(\eta)-z_s}{z-z_s}\right)_{\eta_s}K\right\}$$

$$\text{for } |z_f-z_s|<|z-z_s|<|z_e-z_s|$$

$$=-\frac{\partial y}{\partial\eta}, \quad \text{for } |z-z_s|<|z_f-z_s| \text{ or } |z-z_s|>|z_e-z_s| \tag{6}$$

where

$$z_f=z_s+[w(\eta)-z_s]\sigma_f/x$$

and

$$z_e=z_s+[w(\eta)-z_s]\sigma_e/x \tag{7}$$

C. General Solution

Equation (6) has the general solution

$$\partial y/\partial\eta=[w(\eta)-z]G(\eta)H\{x[w(\eta)-z]\}\exp[F(x,\eta,z)] \tag{8a}$$

where G and H are arbitrary functions and

$$\text{for } |z-z_s|<|z_f-z_s|, \quad F(x,\eta,z)=0 \tag{8b}$$

$$\text{for } |z_f-z_s|<|z-z_s|<|z_e-z_s|,$$

$$F(x,\eta,z)=K\ell n\{\sigma_f[w(\eta)-z_s]/(x-\sigma_f)(z-z_s)\} \tag{8c}$$

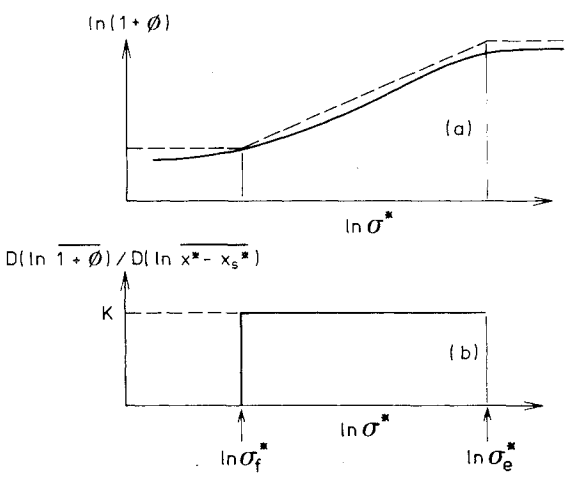

Fig. 3 Reaction rate step function.

and

$$\text{for } |z-z_s|>|z_e-z_s|,$$

$$F(x,\eta,z)=K\{\ell n[\sigma_f(x-\sigma_e)/\sigma_e(x-\sigma_f)]\} \tag{8d}$$

Equation (8a) can be integrated with respect to η to yield

$$y(x,\eta,z)=y_s(x,z)-\int_{\eta}^{\eta_s(x,z)}[w(\eta_1)-z]G(\eta_1)$$

$$\times H\{x[w(\eta_1)-z]\}\exp[F(x,\eta_1,z)]\,d\eta_1 \tag{9}$$

where $\eta_s(x,z)=$const is the trace in the shock where the streamsheet commences. Following Hillier, this equation can be used in conjunction with the body-surface boundary conditions, Eq. (2e), to show that

$$w(\eta)=z_b \tag{10}$$

at the body surface for a detached shock.

The analysis has been general up to this point, applying to configurations in which both the shock wave and the body surface may be curved in both the crossflow plane and the streamwise plane, and the wing leading edges are not necessarily straight, even in planform. The restriction

$$\eta_s(x,z)=z \tag{11}$$

is now applied, implying that, since $w(\eta)=$const on a streamsheet, $\partial y_s/\partial z=$const along all lines $z=$const and the shock profiles in the crossflow plane must be self-similar. As explained by Hillier, it also implies that the wing leading edges lie along lines $z=$const. Thus, with this restriction the analysis is confined to delta planforms with a shock shape that can be derived from a conical form simply by applying streamwise curvature, that is, by applying "simple camber." For such configurations, Hillier showed that, by combining the shock boundary condition (2c) with Eqs. (2b) and (11), it is found that

$$H\{x[w(\eta)-z]\}=H=\text{const} \quad \text{and} \quad G(z)=[w(z)-z]^2/H$$

Equation (9) then becomes

$$y(x,\eta,z)=y_s(x,z)-\int_{\eta}^{z}[w(\eta_1)-z][w(\eta_1)-\eta_1]^{-2}$$

$$\times\exp[F(x,\eta_1,z)]\,d\eta_1 \tag{12}$$

where $F(x,\eta,z)$ is defined in Eqs. (8b-d), with $z_s=\eta$ and with Eqs. (7) used to substitute for z_f and z_e.

Equations (12) provide a means by which solutions can be generated. By choosing a shock shape, $y_s(x,z)$ and $w(\eta)$ are specified, and the integration of Eq. (12) may proceed, by numerical means if necessary. Choice of the shock shape determines the span of the associated wing and hence its planform. This is because, as shown by Messiter for a constant-density flow, the requirement for a sonic component of flow normal to the wing leading edge at the shock reduces to

$$w(\Omega)=1+\Omega \tag{13}$$

Since the density is constant in the present flow close to the shock, where the gas is frozen, the same relation applies here. Integration of Eq. (12) from the shock to the wing surface, which is specified by Eq. (10), then yields the surface shape within the planform corresponding to the chosen shock shape.

III. Approximate Solution Near Wing Midspan

A. Surface Displacement

The foregoing procedure can be followed to determine the effect of reactions on the flow, by taking shock shapes

corresponding to constant-density solutions and determining the changes in the associated surface contours brought about by the reactions. Close to the midspan of the wing, such shock shapes can be represented by the relation[3,4]

$$w(\eta) = a_1 \eta \tag{14}$$

and it is of interest to develop a solution that applies to this region. Also, if $F(x,\eta,z) \ll 1$, that is, if the density changes due to reactions are small, then the approximation

$$\exp [F(x,\eta,z)] \approx 1 + F(x,\eta,z)$$

may be employed and, by making use of Eq. (14), Eq. (12) becomes

$$y(x,\eta,z) = y_s(x,z) + (a_1 - 1)^{-2} \int_\eta^z (a_1\eta_1 - z)\, \mathrm{d}(\eta_1^{-1}) + \int_\eta^z (a_1\eta_1 - z) F(x,\eta_1,z)\, \mathrm{d}(\eta_1^{-1}) \tag{15}$$

The first two terms on the right-hand side of this equation yield the y coordinate for a given streamsheet in constant-density flow. The last term therefore represents the change in y, due to reactions, for that streamsheet, i.e.,

$$\Delta y = (a_1 - 1)^{-2} \int_\eta^z (a_1\eta_1 - z) F(x,\eta_1,z)\, \mathrm{d}(\eta_1^{-1}) \tag{16}$$

Noting the relations (8b-d), Eq. (16) may be written,

$$\text{for } |z-\eta| < |(a_1-1)\eta\sigma_f'|, \qquad \Delta y = 0 \tag{17a}$$

$$\text{for } |(a_1-1)\eta\sigma_f'| < |z-\eta| < |(a_1-1)\eta\sigma_e'|,$$

$$\Delta y (a_1-1)^2 K^{-1} = \int_\eta^{\eta_f} (a_1\eta_1 - z) \{ \ln [\sigma_f'/(1-\sigma_f')] - \ln [(z-\eta_1)/(a_1\eta_1 - z)] \}\, \mathrm{d}(\eta_1^{-1}) \tag{17b}$$

$$\text{for } |z-\eta| > |(a_1-1)\eta\sigma_e'|, \ \Delta y (a_1-1)^2 K^{-1} = \ln [\sigma_f'(1-\sigma_f')/\sigma_e'(1-\sigma_e')] \int_\eta^{\eta_e} (a_1\eta_1 - z)\, \mathrm{d}(\eta_1^{-1}) + \int_{\eta_e}^{\eta_f} (a_1\eta_1 - z) \ln [\sigma_f'(a_1\eta_1 - z)/(1-\sigma_f')(a_1\eta_1 - z)]\, \mathrm{d}(\eta_1^{-1}) \tag{17c}$$

where

$$\sigma' = \sigma/x, \qquad \eta_f = z[1 + (a_1-1)\sigma_f']^{-1}$$

$$\eta_e = z[1 + (a_1-1)\sigma_e']^{-1}$$

Equation (17b) can be written as

$$\Delta y = K(a_1-1)^{-2} \ln [\sigma_f'/(1-\sigma_f')] \{ a_1 \ln (\eta/\eta_f) + z/\eta - z/\eta_f \} - \frac{K}{2(a_1-1)^2} \int_{\eta_1=\eta}^{\eta_1=\eta_f} \left\{ \frac{2a_1}{a_1+1} \left(1 + \frac{a_1-1}{a_1+1} \xi \right)^{-1} - 1 \right\} \times \ln \left(\frac{1+\xi}{1-\xi} \right) \mathrm{d}\xi \tag{18}$$

where $\xi = (a_1-1)^{-1}(2z/\eta_1 - a_1 - 1)$. The condition $\eta_1 = z$ at the shock and Eq. (10) at the body surface ensure that ξ is limited to values between -1 and 1, and therefore it is possible to use the first two terms of the expansion

$$[1 + \xi(a_1-1)/(a_1+1)]^{-1} = 1 - \xi(a_1-1)/(a_1+1) + \xi^2 (a_1-1)^2/(a_1+1)^2 + \cdots \tag{19}$$

to obtain an approximation for the integral in Eq. (18). Integration by parts then yields a solution of Δy. By using Eq. (10) to put $\eta = z/a_1$ in this solution, the displacement of the wing surface toward the shock can be obtained as

$$\Delta y_b K^{-1} = -(a_1-1)^{-2} \{ a_1 \ln a_1 - a_1 + 1 - a_1 \ln [1 + (a_1-1)\sigma_f'] + (a_1-1)\sigma_f' \} \ln [\sigma_f'/(1-\sigma_f')] - (a_1+1)^{-1} \{ \sigma_f' \ln \sigma_f' + (1-\sigma_f') \ln (1-\sigma_f') \} - 2a_1 (a_1+1)^{-2} (1-\sigma_f') \{ 1 + \sigma_f' \ln [\sigma_f'/(1-\sigma_f')] \} \} \tag{20}$$

A similar procedure may be followed with Eq. (17c) to obtain an expression for Δy_b when $|z-\eta| > |(a_1-1)\eta\sigma_e'|$. In writing down this expression, it is convenient to refer to Figs. 2 and 3 to note that $\sigma_e' \gg \sigma_f'$, and thus to simplify it to an approximate form by letting $\sigma_f' \to 0$, obtaining

$$\Delta y_b K^{-1} = -(a_1-1)^{-2} \{ (a_1 \ln a_1 - a_1 + 1) \ln [\sigma_f'(1-\sigma_e')/\sigma_e'] - [a_1 \ln [1 + (a_1-1)\sigma_e'] - (a_1-1)\sigma_e'] \ln [\sigma_e'/(1-\sigma_e')] \} + (a_1+1)^{-1} \{ \sigma_e' \ln \sigma_e' + (1-\sigma_e') \ln (1-\sigma_e') \} + 2a_1 (a_1+1)^{-2} \sigma_e' \{ (1-\sigma_e') \ln [\sigma_e'/(1-\sigma_e')] - 1 \} \tag{21}$$

with maximum error of $0(\sigma_f' \ln \sigma_f')$.

These equations do not involve z, signifying that Δy_b is constant across the span. The manner in which the equations have been developed specifies Δy_b as the displacement of the surface toward the shock wave. It should be noted, however, that Eq. (11) allows the shock wave to adopt any curvature in the streamwise direction and, if the wing surface is fixed, Δy_b can be interpreted as the movement of the shock wave toward the surface.

Δy_b is plotted in Fig. 4a for a wing with a chord sufficient to allow an approach toward a shock layer in chemical equilibrium. Curves are presented for $\sigma_e = 1000\sigma_f$, corresponding to the relaxation profiles for air shown in Fig. 2 and for the range of a_1 associated with the experiments reported later. Reactions begin at $x = \sigma_f$ and first reach equilibrium, at the wing surface, for $x = \sigma_e/\sigma_f$, but it can be seen that nonequilibrium effects continue to be a significant influence for a further increase in chordwise distance by nearly a factor of 10.

By retaining more of the terms in Eq. (19), it is possible to obtain more accurate, but correspondingly more complicated, expressions for Eqs. (20) and (21). When an additional two terms were retained to calculate the curves for $a_1 = 0.5$ and 2 in Fig. 4a, the changes in Δy_b could not be distinguished on the scale of the graph, indicating that Eqs. (20) and (21) are adequate for the range of a_1 shown.

For flight conditions, particular interest centers on chord lengths much greater than σ_f but less than σ_e. A simplified approximate form for $(\Delta y)_b$ may then be obtained by neglecting terms of $0(\sigma_f')$ in Eq. (20), leading to

$$\Delta y_b K^{-1} = -(a_1-1)^{-2} (a_1 \ln a_1 - a_1 + 1) \ln \sigma_f' - 2a_1 (a_1+1)^{-2} \tag{22}$$

Now, as shown by Hida,[4] integration of the second term of Eq. (15) yields

$$\Delta_0 = (a_1-1)^{-2} (a_1 \ln a_1 + 1 - a_1) \tag{23}$$

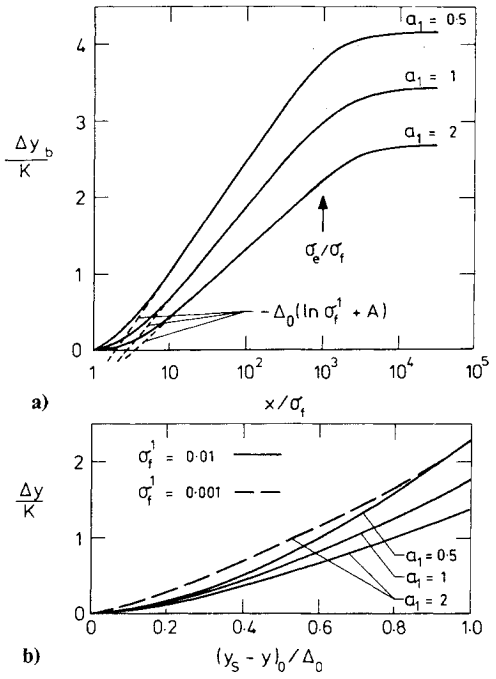

Fig. 4 Effects of reactions as predicted by approximate theory: a) change in centerline shock standoff; b) streamline displacement.

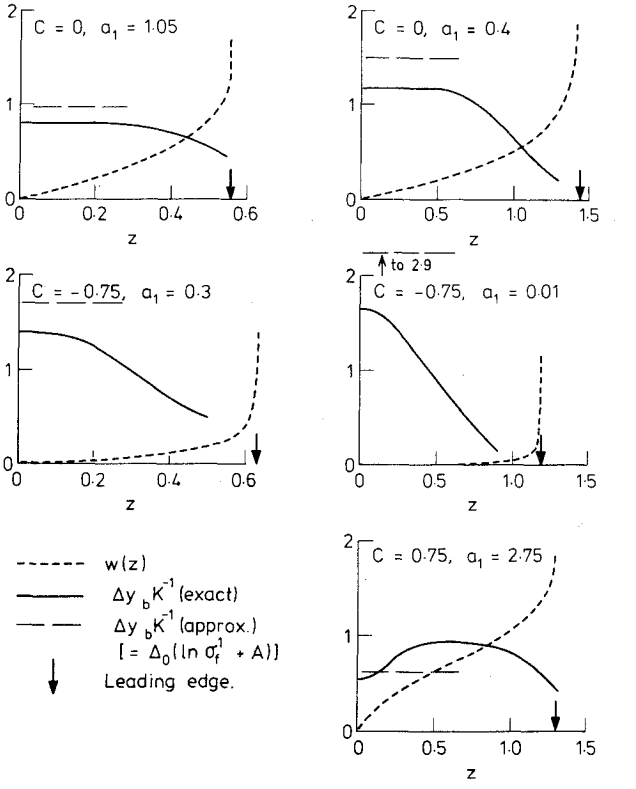

Fig. 5 Wing surface displacement due to reactions—exact and approximate ($\sigma_f' = 0.05$, $K = 0.1$).

where Δ_0 is the constant-density shock standoff distance on the centerline. Therefore Eq. (22) can be written as

$$\Delta y_b = -K\Delta_0(\ell n\sigma_f' + A) \tag{24}$$

where $A = 2a_1(a_1-1)^2(a_1+1)^{-2}(a_1\ell n a_1 + 1 - a_1)^{-1}$.† This approximate equation is also plotted in Fig. 4a and is seen to coincide closely with Eq. (20) in the range of values of x/σ_f that are of interest.

The first term on the right-hand side of Eq. (24) represents the overall increase in average density as reaction lengths in the shock layer are increased by moving downstream; the second term represents the effect on the crossflow pattern of changes in density distribution caused by the reactions. The relative magnitude of the two terms depends upon the distance from the apex as well as the spanwise velocity. At the highest transverse shock curvature, corresponding to $a_1 = 2$, when the spanwise velocity is greatest, A is 0.5 of $\ell n\sigma_f'$ at $\sigma_f' = 0.1$ and falls to 0.25 of $\ell n\sigma_f'$ at $\sigma_f' = 0.01$. For $a_1 = 0.5$, the respective fractions are 0.3 and 0.15.

B. Modification to Crossflow Pattern

The reaction-induced change in the crossflow pattern may be estimated by returning to Eq. (18) and, as before, using the approximation derived from Eq. (19) to evaluate the integral. Then, neglecting terms of $0(\sigma_f')$, it is found that

$$\begin{aligned}\Delta yK^{-1} = &-(a_1-1)^{-2}(a_1\ell n\lambda + 1 - \lambda)\ell n\sigma_f' \\ &-(a_1+1)^{-1}\ell n(a_1-1) + (a_1^2-1)^{-1}[(\lambda-1)\ell n(\lambda-1) \\ &+(a_1-\lambda)\ell n(a_1-\lambda)] + 2a_1(a_1-1)^{-1}(a_1+1)^{-2}\{1-\lambda \\ &+(a_1-1)^{-1}(a_1-\lambda)(\lambda-1)\ell n[(\lambda-1)/(a_1-\lambda)]\}\end{aligned} \tag{25}$$

where $\lambda = z/\eta$. This expression yields the displacement of the streamlines toward the shock and is plotted in Fig. 4b. Integration of the second term of Eq. (15) yields $(y_s - y)_0 = (a_1 - 1)^{-2}(a_1\ell n\lambda + 1 - \lambda)$ for the distance of the streamline from the shock in constant-density flow, and this is used as the abscissa in Fig. 4b. If Δy varies linearly with $(y_s - y)_0$, then the crossflow pattern may be obtained conveniently from the constant-density crossflow pattern by a suitable uniform contraction of the y coordinate. As may be seen from the figure, this is true only to a rough approximation, which is more accurate at the higher than the lower values of a_1. As may be expected, it becomes more accurate as σ_f' is reduced, since the first term in Eq. (25) then becomes more dominant.

C. Comparison with Exact Calculations

In Fig. 5, some sample results of the approximate theory, as summarized in Eq. (24), are compared with exact calculations in which numerical methods were used to perform the integration in Eq. (12) for constant-density shock shapes obtained from Ref. 3. At $C = 0$, corresponding to a flat wing, a midspan region exists in which the exact and approximate theories are consistent, and this region increases with centerline shock curvature. The approximate values of Δy_b are high because the value of K, chosen to be slightly in excess of the highest value associated with the experiments, in fact yields excessive relaxation-induced density changes in Fig. 5 of the order of 30%. It is found that reducing K brings the two theories into closer agreement. At $C = -0.75$, corresponding to a caret wing, the case where $a_1 = 0.01$ shows wide divergence between the two theories, but again, agreement improves as the shock curvature increases with detachment. At $C = 0.75$, corresponding to the diamond cross section, the midspan region of agreement is negligible, but it is interesting to note that, if the measured slope of the $w(z)$ curve between $z = 0.4$ and 0.9 is used for a_1, then Eq. (24) provides a good prediction of Δy_b in this region.

A distinct feature of the results is that, as $w(z)$ deviates from the linear form in approaching the wing leading edge, a contoured and somewhat unrealistic wing shape develops. For constant-density flows, Squire[3] avoided this difficulty by taking more practical surface shapes and using numerical methods to calculate the shock shape. Unfortunately, the

†Note that Eq. (24) is similar to Eq. (17) of Ref. 10, with a more accurate approximation used to obtain the second term.

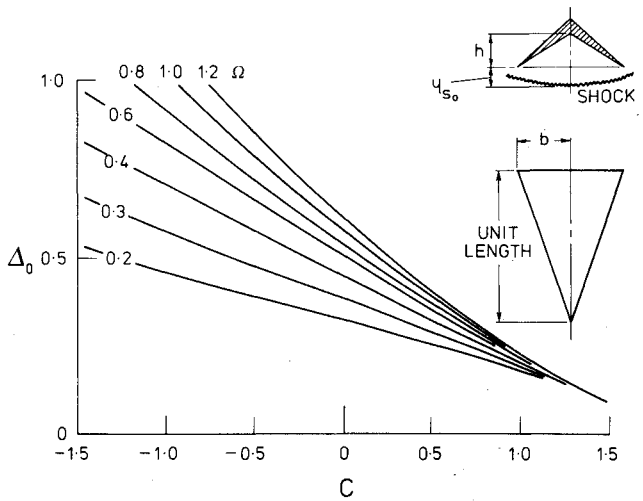

Fig. 6 Centerline shock standoff in constant-density shock layer ($\Delta_0 = y_{s0} + h$, $\Omega = b/(\epsilon^{1/3}\tan\alpha)$, $C = -h/b\epsilon^{1/3}$).

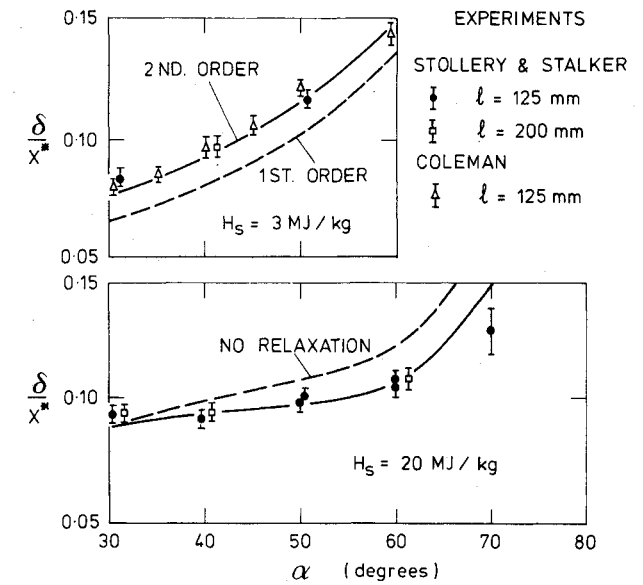

Fig. 7 Shock standoff on flat delta wing—effect of incidence (leading-edge sweep = 75 deg).

theory developed here strictly does not allow this procedure, as the x dependence in Eq. (12) then conflicts with the requirement, expressed in Eq. (11), that the shock profiles in the crossflow plane be self-similar.

It is possible, however, to obtain a rough estimate of the effect of displacing the surface near the wing leading edge to cause it to "straighten." Figure 6 summarizes calculations made by Squire,[3] displaying the effect on constant-density centerline shock standoff of changes in dihedral of a wing with plane surfaces. A Δy_b at the wing tip of 0.1 corresponds to a change in C of the same order and leads to a change in Δ_0 of the order of 0.025. The change is in a direction that tends to bring the exact theory into closer agreement with the approximate theory. Through Eq. (23), this leads to a change of the order of 10% in a_1 and, from Eq. (24), it then follows that changes in Δy_b are of the order of 5%. Thus, both the direct effect of altering C and the indirect effect on $(\Delta y)_b$ remain small in comparison with the wing tip displacement causing C to change. Accepting that changes induced by straightening the surfaces in Fig. 5 will be of the same order as those obtained by changing C, it can be concluded that only a second-order error is made if the approximate solution is assumed to apply to wings with plane surfaces.

IV. Comparison with Experiment

Stollery and Stalker[6,7] performed a series of experiments on delta wings in a free-piston shock tunnel, at test section densities and stagnation enthalpies that allowed effects due to chemical relaxation to be observed in air. They used the schlieren technique to measure the shock standoff at the midspan of the wing and obtained a set of results at a stagnation enthalpy of 20 MJ/kg that may be compared with the predictions made according to the present analysis. The associated test conditions involved a pitot pressure of 70 kNm^{-2} and a Mach number of 7.5.

To calculate the shock standoff, the density immediately after the shock is required. Although the preceding analysis has implicitly used the postshock frozen density for this purpose, there is clearly some arbitrariness about this choice, since, provided the density chosen is reached close to the shock, it will make no physical difference to the flow whether the shock boundary conditions are taken at the frozen values or at values that incorporate some of the relaxation process. It may be expected that any variation in standoff distance arising from this choice will be compensated for in the calculation of Δy_b, and indeed, this has been confirmed numerically for a number of typical cases. When conditions are such that a substantial degree of chemical relaxation occurs within the shock layer, then there is an advantage in choosing a value of density that incorporates some of the relaxation process, since the density changes in the subsequent relaxation are thereby reduced and the small density-change approximation used in arriving at Eq. (24) is correspondingly more accurate. For comparison with the experiments, the density 5 mm downstream of the shock was used, thereby limiting density changes due to relaxation to 20% of the shock density. With the effective shock-density ratio so defined, Fig. 6 can be used to determine a first-order value for the constant-density shock standoff.

The value of shock standoff so obtained must now be corrected for second-order effects associated with constant-density theory. These are discussed in Ref. 10, and are seen to arise from second-order corrections to the y component of velocity immediately after the shock and from the spanwise density gradient induced by the curvature of the shock in the crossflow plane. Arguments are advanced in Ref. 10 which allow approximate expressions to be developed for the change in centerline shock standoff due to each of these effects, thus:

$$(\Delta y)_{0v} = \epsilon y_{s0}\Delta_0(1 + y_{s0}\tan^2\alpha) \tag{26}$$

for the change in standoff due to the postshock velocity correction, and

$$(\Delta y)_{0p} = \epsilon y_{s0} 2a_1 (a_1 - 1)^{-2}[2(a_1 - 1) - (a_1 + 1)\ln a_1] \tag{27}$$

for the spanwise pressure gradient effect. The combined effect of these two corrections is displayed in Fig. 7 as the difference between the first-order and second-order curves at $H_s = 3$ MJ/kg, and they are seen to lead to a satisfactory prediction of constant-density shock standoff.

Finally, the effect of chemical relaxation within the shock layer is estimated from Eq. (24) and added as a further correction to the shock standoff. In order to employ Eqs. (24) and (27) it is necessary to know the appropriate value of a_1. This may be obtained most conveniently by using Fig. 6 to yield the centerline shock standoff distance and coupling this with Eq. (23) to calculate a_1.

The effects of varying incidence with a flat delta wing are shown in Fig. 7. Results are plotted as δ/x^*, the midspan shock stand-off divided by the midspan value of x^*. Low-enthalpy results of gun tunnel experiments by Coleman,[9] as well as those of Stollery and Stalker, are included. The difference between the second-order curve at $H_s = 3$ MJ/kg and the "no-relaxation" curve at $H_s = 20$ MJ/kg is due to the effect of reactions on the effective shock-density ratio. The

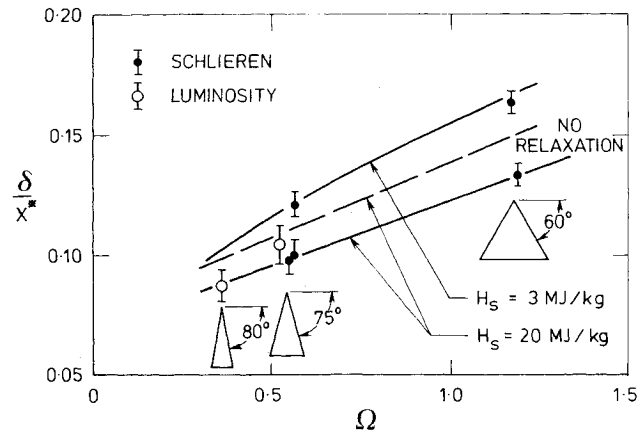

Fig. 8 Shock standoff on flat delta wing—effect of planform [$\alpha = 50$ deg, $l = 200$ mm, $\Omega = b/(\epsilon^{1/2}\tan\alpha)$].

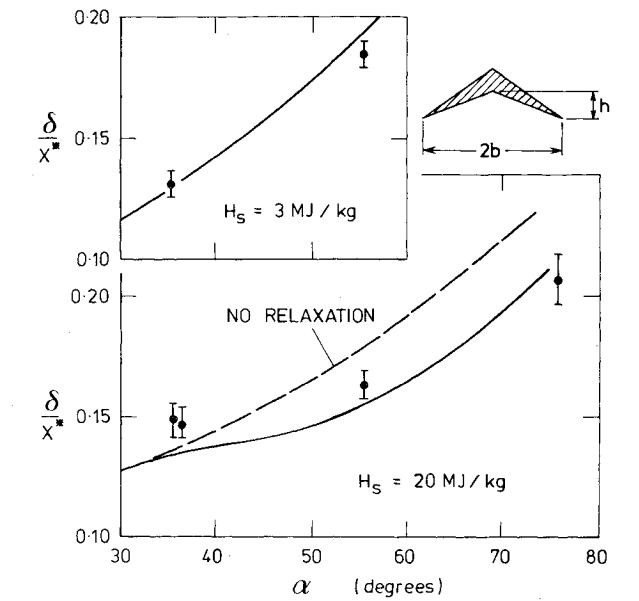

Fig. 9 Shock standoff on caret delta wing—effect of incidence (leading-edge sweep = 75 deg, $h/b = 0.39$, $l = 125$ mm).

experimental point at $\alpha = 70$ deg is also subject to the effects of a subsonic trailing edge. The effect of chemical relaxation can be seen by comparing the two theoretical curves at $H_s = 20$ MJ/kg, as the continuous curve shows the standoff predicted with the relaxation term Δy_b included. The satisfactory agreement between this curve and the experimental results is confirmation that the mismatch between the theoretical requirements for the surface contour near the leading edge and the flat surface provided in the experiments does not have a first-order effect on the flow near the midspan.

This conclusion is reinforced by the results of Fig. 8, involving delta wings of varying aspect ratio at fixed incidence. In Fig. 7, a_1 varied from 0.8 at 40 deg to 1.5 at 60 deg, whereas here it varies from 0.5 to 1.6. The low-enthalpy results shown in the figure confirm the validity of the second-order constant-density corrections as a basis for calculation of the no-relaxation curve at high enthalpy, in spite of the relatively high aspect ratio represented by allowing a leading-edge sweep angle as low as 60 deg. It is clear that the relaxation effect also is satisfactorily predicted at this sweep angle. At the highest sweep angle, lack of schlieren sensitivity unfortunately made it necessary for Stollery and Stalker to revert to luminosity photographs for flow visualization, with some associated loss in accuracy. Thus the significance of the consistency between theory and experiment is somewhat diminished in that case.

Results for the caret wing are presented in Fig. 9. The value of a_1 varies from 0.2 at $\alpha = 55$ deg to 1.3 at $\alpha = 75$ deg, which, according to Fig. 5, implies that there is a significant region near the midspan in which the approximate theory is expected to be valid. There is a slight but systematic discrepancy between experiment and theory in the rate at which standoff increases with increasing incidence. This is evident at both stagnation enthalpy levels and is tentatively ascribed to the fact that, with a wing anhedral angle of 21 deg, the wing surface does not strictly satisfy the requirement of the theory that the surface slope should be small. When an allowance is made for this discrepancy, the variation with incidence of the relaxation-induced decrease in standoff is seen to be in accord with predictions, although the agreement is not as clear cut in this case as it is for the flat wings.

V. Conclusion

The investigation has shown that the effects of density changes due to chemical relaxation in the flow over a delta wing can be accommodated within existing shock layer theory for delta wings. This is possible because the theory essentially involves a conical flowfield and chemical relaxation induces a rate of change of density that is inversely proportional to the streamwise distance from the beginning of the interaction. This effect allows the influence of density changes in a fluid element to remain matched to the expanding scale of a conical flowfield as it passes downstream. An approximate analytic solution has been developed which applies, when density changes are small, to the part of the flow near the midspan. It is consistent with exact numerical calculations for flat and caret delta wings with a shock wave that is well detached, and predicts that the effect of reactions is to displace the shock wave toward the surface without altering its shape. The exact calculations showed that, strictly, somewhat distorted surface shapes are required to accommodate the requirements of the approximate theory. Order-of-magnitude arguments indicated, however, that only second-order errors are made in applying the solutions to more practical wings with plane surfaces. This was confirmed by experiments on flat and caret delta wings.

Acknowledgment

This work is part of a project supported by the Australian Research Grants Committee.

References

[1] Messiter, A. F., "Lift of Slender Delta Wings According to Newtonian Theory," *AIAA Journal*, Vol. 1, April 1963, pp. 794-801.

[2] Hillier, R., "Three Dimensional Wings in Hypersonic Flow," *Journal of Fluid Mechanics*, Vol. 54, Part 2, July 1972, pp. 305-337.

[3] Squire, L. C., "Calculated Pressure Distributions and Shock Shapes on Thick Conical Wings at High Supersonic Speeds," *Aeronautical Quarterly*, Vol. 18, May 1967, pp. 185-205.

[4] Hida, K., "Thickness Effects on the Force on Slender Wings in Hypersonic Flow," *AIAA Journal*, Vol. 3, March 1965, pp. 427-432.

[5] Squire, L., "Some Extensions of Thin-Shock-Layer Theory," *Aeronautical Quarterly*, Vol. 25, Feb. 1974, pp. 1-12.

[6] Stollery, J. L. and Stalker, R. J., "Delta and Caret Wing Measurements in a Hypersonic, High Enthalpy Shock-Tunnel," Imperial College, London, Dept. of Aeronautics Tech. Note 73-104, 1973.

[7] Stalker, R. J. and Stollery, J. L., "The Use of a Stalker-Tube for Studying the High Enthalpy, Non-Equilibrium Airflow over Delta Wings," *Proceedings of the 10th International Shock Tube Symposium*, University of Kyoto Press, Kyoto, Japan, July 1975, pp. 55-66.

[8] Lordi, J. A., Mates, R. E., and Moselle, J. R., "Computer Program for the Numerical Solution of Nonequilibrium Expansions of Reacting Gas Mixtures," NASA CR-472, May 1966.

[9] Coleman, G. T., "Force Measurements on Caret and Delta Wings at High Incidence," Imperial College, London, Dept. of Aeronautics Aero. Rept. 72-16, July 1972.

[10] Stalker, R. J., "Non-Equilibrium Flow over Delta Wings with Detached Shock Waves," AIAA Paper 80-1424, July 1980.